

Characterization of Kerfless Linear Arrays Based on PZT Thick Film

Tomasz Zawada, Louise Møller Bierregaard, Erling Ringgaard, Ruichao Xu, Michele Guizzetti,
Franck Levassort, and Dominique Certon

Abstract—Multielement transducers enabling novel cost-effective fabrication of imaging arrays for medical applications have been presented earlier. Due to the favorable low lateral coupling of the screen-printed PZT, the elements can be defined by the top electrode pattern only, leading to a kerfless design with low crosstalk between the elements. The thick-film-based linear arrays have proved to be compatible with a commercial ultrasonic scanner and to support linear array beamforming as well as phased array beamforming. The main objective of the presented work is to investigate the performance of the devices at the transducer level by extensive measurements of the test structures. The arrays have been characterized by several different measurement techniques. First, electrical impedance measurements on several elements in air and liquid have been conducted in order to support material parameter identification using the Krimholtz–Leedom–Matthaei model. It has been found that electromechanical coupling is at the level of 35%. The arrays have also been characterized by a pulse-echo system. The measured sensitivity is around -60 dB, and the fractional bandwidth is close to 60%, while the center frequency is about 12 MHz over the whole array. Finally, laser interferometry measurements have been conducted indicating very good displacement level as well as pressure. The in-depth characterization of the array structure has given insight into the performance parameters for the array based on PZT thick film, and the obtained information will be used to optimize the key parameters for the next generation of cost-effective arrays based on piezoelectric thick film.

Index Terms—Kerfless, Krimholtz–Leedom–Matthaei (KLM) model, linear array, PZT thick film, screen printing, ultrasonic transducer.

I. INTRODUCTION

TREMENDOUS increase of computational power and miniaturization of portable devices as well as preference for wireless solutions are currently driving the development in the next generation of ultrasonic diagnostic instrumentation [1], [2]. At the same time, the imaging quality depends on the quality of the ultrasonic transducer that still constitutes the main component of every ultrasonic system. On the other hand, many new products require special attention to costs not

only at the production level but also even at the prototyping phase. Therefore, transducer quality needs to be accompanied by the cost-effectiveness of the solution in order to truly enable excellent imaging quality as well as breakthrough cost reduction.

Currently, a few major trends in medical ultrasound transducers are noticeable [3]. A significant effort goes into the development of capacitive micromachined ultrasonic transducer (cMUT) [4], but this solution is mainly suitable for high-volume products due to the need for very high upfront investments. Moreover, the variety of different medical conditions calls for a relatively large number of different transducer types, which is contrary to the paradigm of mass produced silicon devices. The large upfront investment of cMUT technology is greatly limiting the accessibility for small organizations that are known to drive new innovative products and technologies.

Another trend, especially in higher frequency applications (above 20 MHz) is to down-scale the 2-2 composite technology combined with a heterogeneous integration approach. There are a number of reports where elements have been stacked [5], diced [6], [7], or etched using deep reactive ion etching [8]–[10] out of bulk or film material. However, in many cases the higher integration level as well as higher element counts leads to significantly more complex processes that in turn greatly increase the costs of production.

A rather different fabrication principle is to use one of the methods collectively known as rapid prototyping, where the transducer is built up in free form based on a 3-D CAD file [11]. This has the advantage of freedom of shaping; however, the resolution is still a limiting factor.

There are also reports on solutions where the elements are defined by the electrode pattern (kerfless design) rather than by dicing, leading to significant simplification of the production process hence reducing production costs [12], [13]. However, in many cases the kerfless design compromises significantly the electroacoustic properties of the transducer (e.g., crosstalk) [13]. In this paper, however, we present that due to the anisotropic nature of screen-printed PZT films (large difference between thickness and lateral coupling) the kerfless design does not necessarily need to lead to compromised crosstalk between the elements.

The detailed description of a cost-effective solution based on screen printed multielement arrays has been published earlier [14], and the main objective of the presented work is to investigate deeper the electroacoustic properties of PZT thick-film-based acoustic arrays in order to aid the future design

Manuscript received January 6, 2017; accepted May 22, 2017. Date of publication May 26, 2017; date of current version August 28, 2017. This work was supported by the Innovation Fund Denmark through platform project “FutureSonic” under Contract 82-2012-4. (Corresponding author: Tomasz Zawada.)

T. Zawada was with Meggitt Sensing Systems, 3490 Kvistgaard, Denmark. He is now with TOOsonix A/S, 2970 Hoersholm, Denmark (e-mail: tomasz.zawada@toosonix.com).

L. M. Bierregaard, E. Ringgaard, R. Xu, and M. Guizzetti are with Meggitt Sensing Systems, 3490 Kvistgaard, Denmark (e-mail: erling.ringgaard@meggitt.com).

F. Levassort and D. Certon are with the GREMAN UMR 7347 CNRS, University of Tours, 37100 Tours, France (e-mail: franck.levassort@univ-tours.fr).

Digital Object Identifier 10.1109/TUFFC.2017.2709253

and optimization of similar structures. It has to be emphasized that the applied process is characterized by relatively low manufacturing costs as well as prototyping costs.

It is envisaged that the presented solution can serve as a platform for several applications that might benefit from the combination of low cost, medium to high operating frequency, good sensitivity, and kerfless design. The presented devices operate at 12 MHz; however, the technology enables relatively easy fabrication of devices operating at much higher frequencies (above 50 MHz). Therefore, it can be applied in dermatology, ophthalmology, imaging of small animals, or nondestructive testing.

This paper starts with an introduction to PZT thick-film technology. Then, the test structures of multielement transducers are presented. This is followed by electric and electroacoustic measurements using several techniques including impedance characterization combined with Krimholtz–Leedom–Matthaei (KLM) modeling, laser interferometry as well as hydrophone characterization. Test results are then summarized together with an outlook for the future development.

II. PZT THICK-FILM TEST STRUCTURES

The test structures have been fabricated using PZT thick-film technology [14] based on TF2100 material by Meggitt A/S [15]. This material enables fabrication of highly integrated devices where the active layer is deposited and processed with the substrate and electrode materials. It also offers great flexibility when it comes to patterning methods. Another advantage is high electromechanical coupling combined with relatively high bandwidth.

The transducer consists of an acoustically matched ceramic substrate, on which electrodes as well as the active PZT layer have been printed in consecutive steps. The thickness of the PZT layer corresponding to a center frequency of the transducer of around 12 MHz has been experimentally determined to be equal to $80\ \mu\text{m}$. The PZT thick films were then sintered at temperatures above $800\ ^\circ\text{C}$.

The transducers have been fabricated using a screen-printing technique, where the gold bottom electrode has been deposited first, followed by deposition of the TF2100 PZT thick film. The top electrodes defining the elements of the array have been printed as well using silver fine line patterning. The pattern of the top electrode defines the 32-element array. A schematic cross section of the fabricated device is given in Fig. 1. The effective length of the elements is 4.5 mm.

The structures have been poled at elevated temperature using an electric field of $10\ \text{kV/mm}$.

In the presented solution, the top electrode pattern has been designed to match the pattern of conductive pads on a PCB carrier with an opening enabling acoustic coupling to the medium (Fig. 2). As a final step, a polymeric (Parylene) quarter-wave matching layer has been added. A photograph of the fabricated structure is given in Fig. 3. A summary of the geometrical specifications is given in Table I.

Typically, the packaging and interconnect of multielement transducers is one of the major technical challenges when

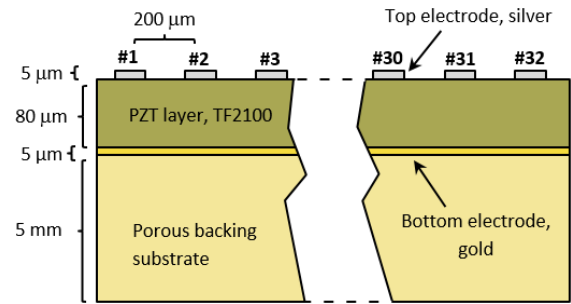


Fig. 1. Schematic cross section of the fabricated multielement transducer (not to scale).

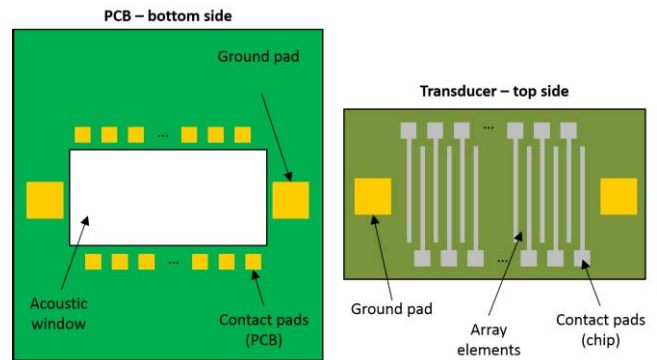


Fig. 2. Schematic illustration of the applied packaging technique. The transducer chip is mounted upside down onto the PCB using flip-chip technology (not to scale).

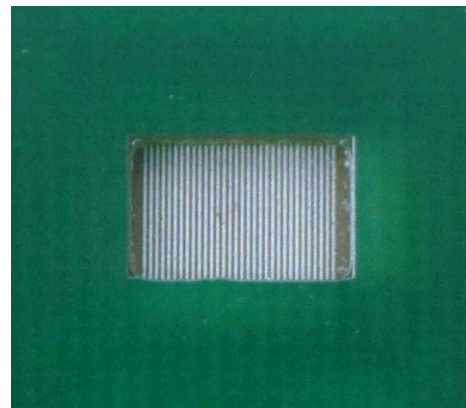


Fig. 3. Top-view close-up of a PCB-packaged 32-element transducer.

it comes to design and manufacturing of array devices. The presented solution is based on the flip-chip technique where the functional device (chip) is connected to the PCB using solder bumps deposited on the top of the device. Hence, the device is finally attached “upside down” with the active side facing the PCB.

It must be noted that the chosen element width of the array has been dictated by the technological limitations of the patterning technique (screen printing). Even though widths of $20\ \mu\text{m}$ are achievable with fine line screen-printing techniques, the width of $80\ \mu\text{m}$ has been chosen to ease the fabrication and enable further characterization, as this work was a part of a feasibility study. As will be shown later, $80\ \mu\text{m}$ width corresponds to $160\ \mu\text{m}$ effective aperture of an element,

TABLE I
SUMMARY OF THE GEOMETRICAL SPECIFICATION OF
THE TEST STRUCTURES

Number of elements	32
Element pitch	200 μm
Element width	80 μm
Element length	4.5 mm

which works very well for a pitch of 200 μm as designed. Due to those constraints, the operating frequency was chosen to be at 12 MHz, which is in the lower end of the achievable range of screen-printed PZT, yielding a pitch of 1.5λ .

III. CHARACTERIZATION OF THE TEST DEVICES

This section aims to provide a set of electromechanical characteristics of the fabricated arrays. At this step of the technology development, it has been chosen to focus investigations on the elementary performance of the transducer. Sections III-A and III-B present standard electromechanical measurements, i.e., electrical impedance and pulse-echo characterization. Sections III-C and III-D are dedicated to the characterization of the emitted pressure with two objectives: 1) to assess the emitted pressure amplitude in pulsed mode with hydrophone and 2) to evaluate the impact of mechanical crosstalk from element to element on the transducer directivity. For this, it was chosen to use laser interferometry measurements performed on the front face of the transducer when loaded with water. The background of these investigations was two fundamental questions. The first concerns identification of elastic guided modes in the structure, since one of the special features of the device is that elements are not subdiced, contrary to standard technology. It is well-known that guided modes, if they are radiated, can create significant degradation of the final image. The second is to assess the real mechanical aperture of the transducer. As explained in the previous part, elements are defined by electrode patterning only, i.e., width and pitch. However, it is clear that the electrical aperture defined by electrode width is not the aperture that must be used to predict the final radiation pattern of the probe. Since there is no mechanical discontinuity from element to element, the real aperture of the element is inevitably larger than the one defined by the electrode width.

A. Impedance Spectra and KLM Modeling

The electromechanical properties of the PZT thick films were deduced from the measurements of the complex electrical impedance around the fundamental thickness-mode resonance. An E4990A spectrum analyzer (Keysight Technologies Inc., Palo Alto, CA, USA) and an impedance test kit (Keysight 42941A) were used as the experimental setup. In order to reduce the influence of the interconnect, measurements were carried out on a chip-level device (without matching layer), as depicted in Fig. 4.

The theoretical behavior of the electrical impedance was computed as a function of frequency for the thickness-mode

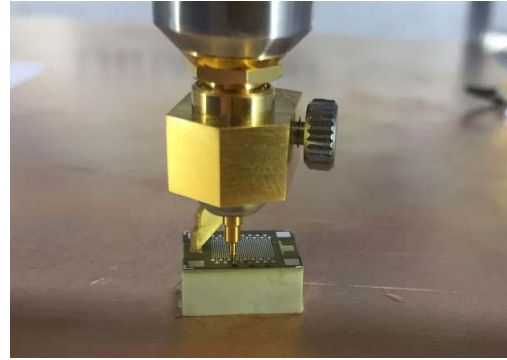


Fig. 4. Chip level impedance characterization setup.

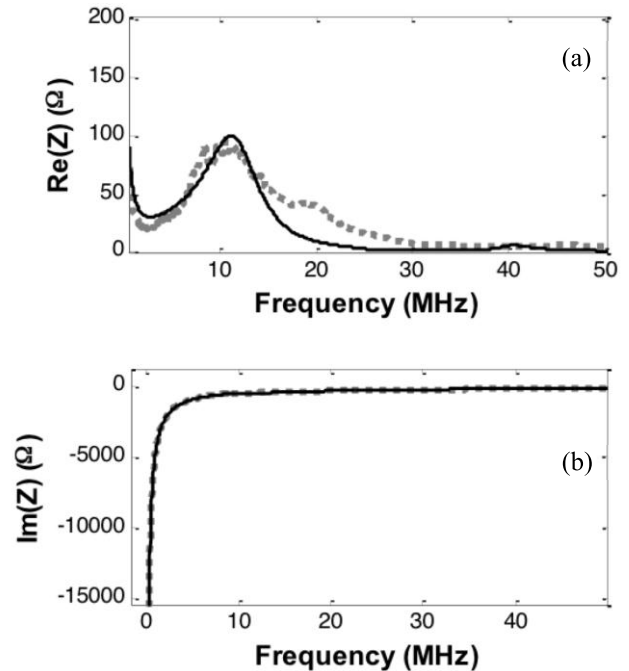


Fig. 5. Complex electrical impedance in air [(a) real part and (b) imaginary part] (element 8) as a function of frequency (dashed gray lines: measurement; solid black lines: theoretical using KLM model).

using a 1-D model based on the KLM equivalent electrical circuit [16]–[18]. A fitting process was then used to deduce the thickness-mode parameters of the PZT thick films from the experimental data.

The considered structures of all samples were composed of a piezoelectric layer and three inert layers with the porous substrate and two electrodes (gold for bottom electrode and silver for top electrode with a thickness of around 5 μm for each). For the porous PZT backing, according to the porosity content, the acoustical impedance used was estimated at 13.2 MRa [19]. The parameters of these layers were fed into the KLM model and considered as constants. Finally, five thickness-mode parameters of the thick films were deduced: the longitudinal wave velocity c_L , the dielectric constant at constant strain, the effective thickness coupling factor k_t , and the loss factors (mechanical δ_m and electrical δ_e). The electrical impedance of several elements was measured in order to verify good reproducibility. Fig. 5 represents the

TABLE II
ESTIMATED PZT THICK-FILM PARAMETERS
ACCORDING TO KLM MODEL

Parameter	Symbol	Value
Effective thickness coupling factor	k_t (%)	35
Mechanical loss factor	δ_m (%)	6
Electrical loss factor	δ_e (%)	0.5
Dielectric permittivity constant strain	$\epsilon_{33}^S/\epsilon_0$	550
Longitudinal wave velocity	c_L (m/s)	2900
Thick film resonance frequency (in free mechanical conditions)	f_0 (MHz)	17

electrical impedance in air of one representative element (#8) as a function of frequency. Here, the porous PZT substrate fulfills the standard conditions of a backing structure (i.e., the acoustical attenuation and thickness of this element are sufficiently high to be considered as a semi-infinite medium). In this case only, the standard fundamental resonance is observed [20].

If this was not the case, the backing would constitute an additional layer acting as a coupled resonator with the piezoelectric thick film. Thus, multiple peaks would be observed on the electrical impedance [21]. The extracted parameters are summarized in Table II. According to the previous study [22] on similar structures, error measurements were estimated for k_t at $\pm 1.5\%$ and for mechanical losses at $\pm 2\%$.

Electrical impedance measurements were performed for all 32 elements and two different arrays in [14]. Good reproducibility was observed on capacitance distribution with a relative variation less than 4%. For the present array, five measurements were performed on elements #1, #8, #16, #24, and #32 which are regularly distributed on the structure. Results show very close electromechanical properties, in particular for k_t with $35\% \pm 1\%$. Moreover, resonance frequency is uniformly distributed at 17 MHz (in free mechanical conditions) showing a homogeneous microstructure and uniform thickness of the piezoelectric thick film.

B. Pulse-Echo Characterization

Several elements of the linear array have been characterized with a metallic target in water at 3.5 mm. An Olympus (model 5077PR, Rungis, France) square wave pulser/receiver was used for the electrical excitation and reception with a sampling frequency at around 200 MHz. A 50- Ω cable around 50 cm in length was used. Fig. 6 represents the pulse-echo response of the element number 16.

The insertion loss (IL) = $20 \log(U_r/U_e)$, where U_r and U_e are the reception and excitation peak voltages, has been evaluated from the received voltage in pulse-echo mode and found to be equal to -60 dB for a center frequency at 12 MHz. The fractional bandwidths have been found at -6 and -20 dB to be 41% and 106%, respectively. The reproducibility of

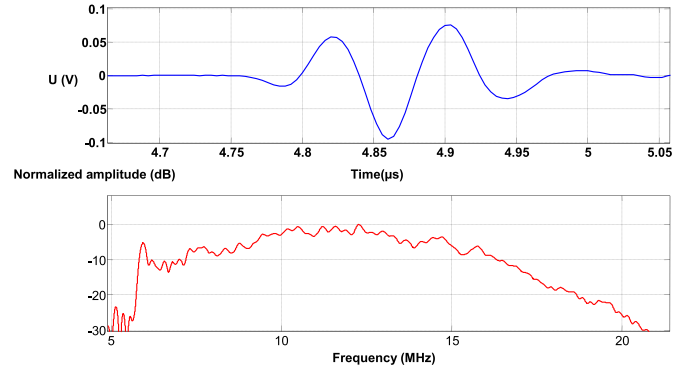


Fig. 6. Pulse-echo response in time and frequency domain (element 16).

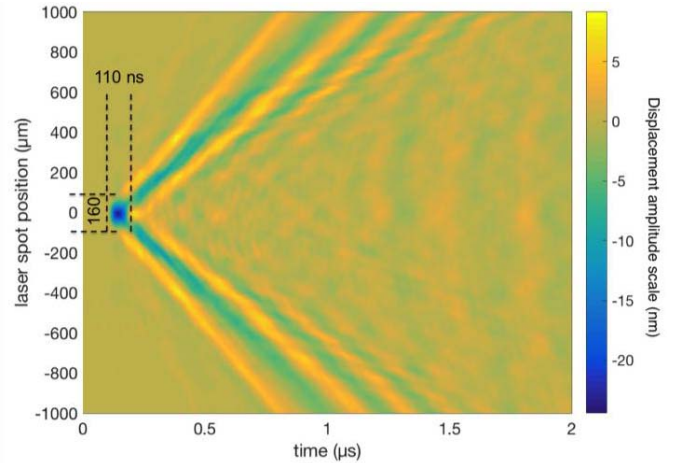


Fig. 7. Scan of the displacement in water collected at the surface of the array when one element is electrically excited.

these parameters was previously checked [14] with a typical standard deviation of 2.6 dB on the sensitivity.

C. Displacement Measurements

The mechanical displacement at the surface of the array, loaded with water, produced by excitation of one element was measured using laser interferometer (apparatus UHF-120 from Polytec SA, Waldbronn, Germany). The displacement has been scanned along a line placed at the center of the elevation, with a step of 20 μm , over a range of 2 mm from either side of the excited element. The pitch was chosen small enough to measure the real mechanical aperture with good resolution, and the scanned surface was large enough to measure correctly the contribution of guided modes along the array. Electrical excitation conditions were the same as the ones used for pulse-echo experiments. Fig. 7 shows the obtained displacement scan. The small blue spot placed at zero laser spot position corresponds to the displacement measured on the excited element, i.e., this corresponds to the real mechanical aperture. Outside of this spot, the displacement produced on neighboring elements is the mechanical crosstalk caused by guided modes. Fig. 7 points out two interesting features. First, the amplitude of the displacement measured on the

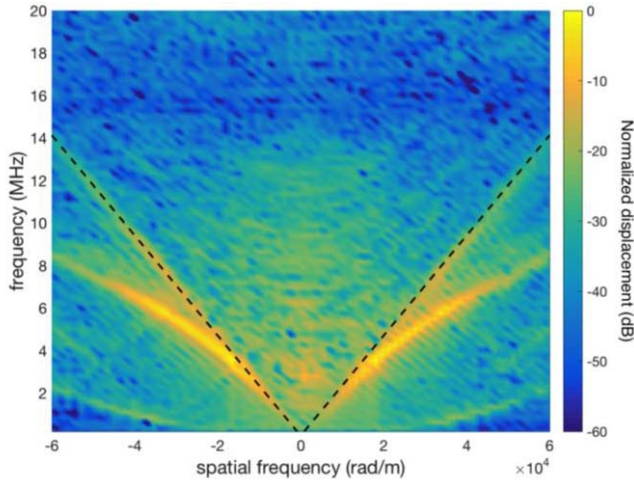


Fig. 8. Plane wave decomposition of the displacement field measured on the array front face. The two dashed black lines correspond to waves with phase velocity of 1480 m/s.

excited element reaches 20 nm, which is quite significant, given the fact that the element has been fabricated using printing technology. Second, the width of the blue spot allows assessing the real mechanical aperture of a single element, which is approximately 160 μm . As expected this value is higher than the electrode width but this is perfectly satisfactory with regards of the array pitch (200 μm).

It can be noted that the pulse duration is short (110 ns), this confirms the high level of damping obtained with the porous backing.

To identify guided modes, the plane wave decomposition, the so-called ω - k diagram, of the measured displacement field was computed (Fig. 8) as explained in [25]. It is recalled that for a given point of the diagram characterized by a frequency ω_0 and wave vector k_0 , there exists a plane wave in the fluid that propagates at angle θ from the normal axis of the array given by the relation $\sin \theta = (k_0/\omega_0) \cdot v_{\text{water}}$, where v_{water} (1480 m/s) is the fluid acoustic velocity. So, only waves for which the phase velocity $v_\phi = \omega_0/k_0$ is higher than v_{water} are propagated in the medium. The others remain confined at the fluid/water interface without contributing to the far-field radiation pressure of the array. The limit between the domains of radiated waves and evanescent waves is marked by the two straight lines with a slope of 1480 m/s. Here, one guided mode with phase velocity lower than 1480 m/s can be clearly observed. This mode explains the mechanical crosstalk measured from element to element. It probably corresponds to the first symmetric Lamb mode of the piezoelectric substrate, but here, in comparison with a bare piezoelectric plate, its phase velocity is strongly modified and decreased by the coupling with the porous backing. The advantage of the porous backing is again clearly confirmed since it allows rejecting guided modes of the plate in the domain of the evanescent plane waves, thus eliminating their contribution to the pressure field directivity. These modes of course constitute a loss of radiated energy, but this is a good technological tradeoff. Moreover, the amplitude of the guided mode, and therefore

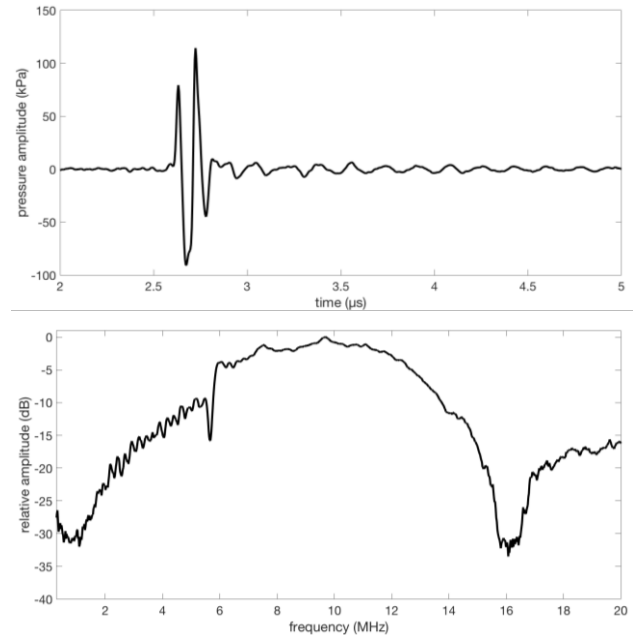


Fig. 9. Pressure measured at 40 mm from the array time response (top) and spectrum (bottom). The central frequency at -3 dB is 9.5 MHz and the corresponding fractional bandwidth is 55%.

mechanical crosstalk, is here overestimated by acousto-optic interactions as explained in [23]. This phenomenon modifies the amplitude of measured displacement with a factor that depends on the phase velocity of propagated waves. For the guided wave observed here, when looking at acousto-optic filter curves given in [23], one can estimate that the ratio between the measured displacement amplitude and the real value is close to 1.33, i.e., the optical index of water.

It should be noted that the measured displacement field could have been corrected by applying an inverse filter of acousto-optic interactions. However, as explained in [23], this solution creates artifacts, adds a virtual mode with phase velocity close to 1700 m/s and causes a degradation of measurement quality in terms of signal-to-noise ratio. It is better to apply the inverse filter to pressure data obtained numerically from the displacement data, in order to provide calibrated pressure amplitude values. Moreover, in the case of arrays with large angular directivity, like phased arrays, correction of acousto-optic effects is mandatory to obtain correct values of beamwidth, but clearly it is not essential for linear arrays [23].

D. Hydrophone Measurements

The pressure field radiated by one element has been characterized by using a hydrophone setup (Calibrated Needle hydrophone, HN series from Onda Corporation, Sunnyvale, USA). Excitation conditions were kept similar to those described in the previous section. In the first step, the far-field pressure emitted (at 40 mm from the array) was measured and the results are presented in Fig. 9.

The central frequency has been found to be equal to 9.5 MHz with a corresponding fractional bandwidth of 55% at -3 dB. One can note the significant peak-to-peak amplitude

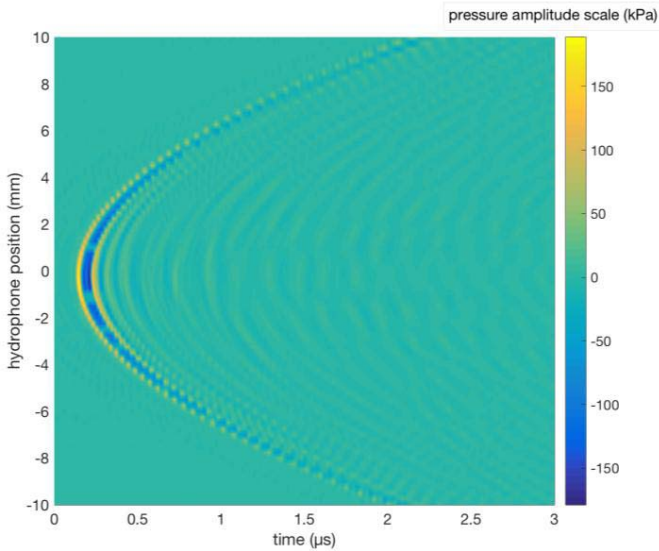


Fig. 10. Pressure measured along line parallel to the array at a distance of 4 mm.

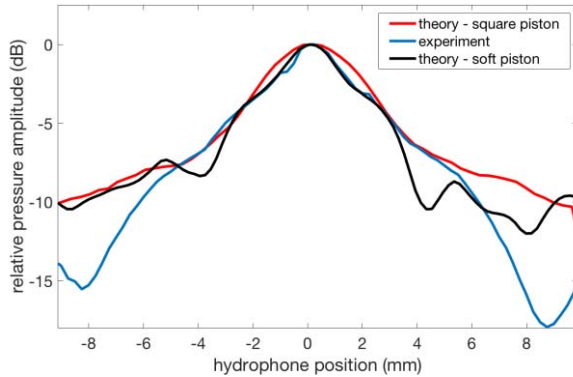


Fig. 11. Variations of the peak-to-peak amplitude against hydrophone position along a line parallel to the array, at distance of 4 mm. The theoretical “soft piston” is the directivity diagram obtained from experimental data of displacements, and the theoretical “square piston” is the curve obtained by assuming the element vibrates like an ideal flat piston.

of the pressure, close to 200 kPa for one element. In comparison with the pulse-echo measurements, the central frequency seems lower in emission. This is due to the existence of a strong cutoff frequency at 16 MHz that is not observed on the pulse-echo signal. As confirmed experimentally, this was due to the difference in coax cable length used in the two experiments. For pulse-echo measurements a 50 Ω cable of 50-cm length was used, while for hydrophone measurements a longer cable (1.5 m) was required.

In the second step, a scan of the pressure at 4 mm from a selected element along a line parallel to the array has been performed. The hydrophone was mechanically moved with a step of 250 μm . Results are presented in Fig. 10. One can note the pressure amplitude at the probe output: more than 300 kPa peak-to-peak (at 10 MHz) for one emitter only. This value is quite significant and comparable with the performance of commercially available probes.

Fig. 11 presents a pressure scan illustrating the variation of the peak-to-peak amplitude against the hydrophone position.

Since the hydrophone cannot be considered a point receiver, the radiated pressure field at 4 mm from the array has been computed using the experimental displacement data, as presented in [23]. The resulting directivity diagrams are plotted in Fig. 11 (black and blue curves). From -4 to $+4$ mm, within amplitude range of $+10$ dB, the two curves are superimposed, which indicates very good agreement of the theoretical analysis with experimental pressure data. The difference observed for hydrophone position beyond the ± 4 mm range can be attributed to the hydrophone head size that has not been considered here in the model of the pressure field.

The theoretical directivity diagram when the element is a flat piston of 160 μm width was simulated as well (red curve in Fig. 11) and compared with the two others. Again, this curve matches well with the two others within the range -4 to $+4$ mm. This means that the elementary directivity pattern is only slightly affected by mechanical crosstalk inside the structure and that its contribution in the far-field is negligible. Note that from -2 to $+2$ mm a small discrepancy between the directivity diagram obtained from the “flat piston” source and the one obtained from experimental data can be observed. This is easily explained by the true shape of the element vibration that is curved and not square, which leads to a slight narrowing of the elementary aperture of the probe.

IV. CONCLUSION

Ultrasonic transducer arrays with 32 elements have been successfully manufactured using a kerfless PZT thick-film technology, and functional characterization of the test devices has been carried out using a number of experimental and analytical methods.

Several material parameters of the PZT thick film have been identified using the KLM model. A reasonably good fit between the experimental and analytically calculated impedance spectra has been obtained. The electromechanical thickness coupling coefficient has been determined to be equal to 35%, which is comparable with some of the previously published data [24].

Impedance measurements show good uniformity throughout the arrays, and pulse-echo measurements yield a quite respectable IL of -60 dB. The corresponding center frequency is equal to 12 MHz, and fractional bandwidths are 41% and 106% at -6 and -20 dB, respectively.

The displacement at the surface of the array measured by laser interferometry is approximately 20 nm. Furthermore, interferometry measurements have confirmed that the mechanical crosstalk between the elements is low and the short pulse duration of 110 ns indicates that the porous backing provides proper damping.

Measurements with a needle hydrophone show a peak-to-peak acoustic pressure as high as 300 kPa at 10 MHz. Moreover, the good agreement between the peak-to-peak amplitude variation with hydrophone position and simulated curves confirms once more that the level of mechanical crosstalk inside the structure is relatively low, and that its contribution in the far-field is low as well.

The comparison between the “soft” and “hard” piston model gives a deeper insight into the mechanics of a single element.

It indicates that the material between the elements due to the kerfless design is providing additional clamping on the side of the element resulting in a narrower pressure distribution.

In conclusion, the characterization shows that the performance of the thick-film arrays is comparable to state-of-the-art commercial transducers. It is worth noting that this is obtained with a technology characterized by low upfront investments, yet allowing up-scaling and manufacturing at very competitive price.

An important task for future work will be to further increase the number of elements. Even though the basic imaging functionality using a commercial scanner has already been demonstrated [14], the significantly enhanced image quality resulting from a higher number of elements will make the presented technology even more competitive to today's state-of-the-art solutions.

ACKNOWLEDGMENT

The authors would like to thank D. Gross and A. Boulmé from GREMAN Laboratory, University of Tours, for their help and skills in the realization of interferometry and hydrophone measurements.

REFERENCES

- [1] T. L. Szabo, *Diagnostic Ultrasound Imaging: Inside Out*, 2nd ed. Oxford, U.K.: Academic, 2014, pp. 366–369.
- [2] M. Lewandowski, K. Siewicz, and M. Walczak, "A low-cost 32-channel module with high-speed digital interfaces for portable ultrasound systems," in *Proc. IEEE Int. Ultrason. Symp.*, Oct. 2012, pp. 1–4.
- [3] K. K. Shung, J. M. Cannata, and Q. Zhou, "High-frequency ultrasonic transducers and arrays," in *Piezoelectric and Acoustic Materials for Transducer Applications*, vol. 21. A. Safari and E. K. Akdogan, Eds., New York, NY, USA: Springer, 2008, pp. 431–452.
- [4] B. T. Khuri-Yakub and Ö. Oralkan, "Capacitive micromachined ultrasonic transducers for medical imaging and therapy," *J. Micromech. Microeng.*, vol. 21, no. 5, pp. 054004–054014, May 2011.
- [5] T. A. Ritter, T. R. Shrout, R. Tutwiler, and K. K. Shung, "A 30-MHz piezo-composite ultrasound array for medical imaging applications," *IEEE Trans. Ultrason., Ferroelectr., Freq. Control*, vol. 49, no. 2, pp. 217–230, Feb. 2002.
- [6] C. T. Chiu, J. A. Williams, B. J. Kang, T. Abraham, K. K. Shung, and H. H. Kim, "Fabrication and characterization of a 20 MHz microlinear phased array transducer for intervention guidance," in *Proc. IEEE Ultrason. Symp.*, Sep. 2014, pp. 2121–2124.
- [7] H.-C. Yang *et al.*, "Low cross-talk kerfless annular array ultrasound transducers using 1–3 piezocomposites with pseudo-random pillars," in *Proc. IEEE Ultrason. Symp.*, Oct. 2012, pp. 1560–1563.
- [8] D. W. Wu, Q. F. Zhou, K. K. Shung, C. G. Liu, and F. T. Djuth, "High-frequency piezoelectric PZT film micromachined ultrasonic arrays," in *Proc. IEEE Ultrason. Symp.*, Nov. 2008, pp. 1222–1225.
- [9] Q. Zhou, D. Wu, C. Liu, B. Zhu, F. Djuth, and K. K. Shung, "Micro-machined high-frequency (80 MHz) PZT thick film linear arrays," *IEEE Trans. Ultrason., Ferroelectr., Freq. Control*, vol. 57, no. 10, pp. 2213–2220, Oct. 2010.
- [10] T. Cummins, P. Eliaho, and K. K. Shung, "High-frequency ultrasound array designed for ultrasound-guided breast biopsy," *IEEE Trans. Ultrason., Ferroelectr., Freq. Control*, vol. 63, no. 6, pp. 817–827, Jun. 2016.
- [11] A. Safari and E. K. Akdogan, "Rapid prototyping of novel piezoelectric composites," *Ferroelectrics*, vol. 331, no. 1, pp. 153–179, 2006.
- [12] C. E. Morton and G. R. Lockwood, "Evaluation of kerfless linear arrays," in *Proc. IEEE Ultrason. Symp.*, Oct. 2002, pp. 1257–1260.
- [13] R. Chen *et al.*, "PMN-PT single-crystal high-frequency kerfless phased array," *IEEE Trans. Ultrason., Ferroelectr., Freq. Control*, vol. 61, no. 6, pp. 1033–1041, Jun. 2014.
- [14] L. M. Bierregaard *et al.*, "Cost-effective screen printed linear arrays for medical imaging fabricated using PZT thick films," in *Proc. IEEE Ultrason. Symp.*, Oct. 2015, pp. 109–112.
- [15] *Datasheet TF2100*, accessed on Apr. 6, 2017. Available: <http://insensor.com/download/files/1234182533.pdf>
- [16] R. Krimholtz, D. A. Leedom, and G. L. Matthaei, "New equivalent circuits for elementary piezoelectric transducers," *Electron. Lett.*, vol. 6, no. 13, pp. 398–399, Jun. 1970.
- [17] S. J. H. Van Kervel and J. M. Thijssen, "A calculation scheme for the optimum design of ultrasonic transducers," *Ultrasonics*, vol. 21, no. 3, pp. 134–140, 1983.
- [18] M. Lethiecq, F. Patat, L. Pourcelot, and L. P. Tran-Huu-Hue, "Measurement of losses in five piezoelectric ceramics between 2 and 50 MHz," *IEEE Trans. Ultrason., Ferroelectr., Freq. Control*, vol. 40, no. 3, pp. 232–237, May 1993.
- [19] P. Marechal, F. Levassort, J. Holc, L. P. Tran-Huu-Hue, M. Kosec, and M. Lethiecq, "High-frequency transducers based on integrated piezoelectric thick films for medical imaging," *IEEE Trans. Ultrason., Ferroelectr., Freq. Control*, vol. 53, no. 8, pp. 1524–1533, Aug. 2006.
- [20] A. Guioy *et al.*, "Dual-frequency transducer for nonlinear contrast agent imaging," *IEEE Trans. Ultrason., Ferroelectr., Freq. Control*, vol. 60, no. 12, pp. 2634–2644, Dec. 2013.
- [21] M. Lukacs, T. Olding, M. Sayer, R. Tasker, and S. Sherrit, "Thickness mode material constants of a supported piezoelectric film," *J. Appl. Phys.*, vol. 85, no. 5, pp. 2835–2843, 1999.
- [22] A. Bardaine, P. Boy, P. Belleville, O. Acher, and F. Levassort, "Improvement of composite sol-gel process for manufacturing 40 μm piezoelectric thick films," *J. Eur. Ceramic Soc.*, vol. 28, no. 8, pp. 1649–1655, 2008.
- [23] D. Certon, G. Férin, O. Boumatar, J. P. Remenieras, and F. Patat, "Influence of acousto-optic interactions on the determination of the diffracted field by an array obtained from displacement measurements," *Ultrasonics*, vol. 42, no. 1, pp. 465–471, 2004.
- [24] D.-W. Wu, Q. Zhou, X. Geng, C.-G. Liu, F. Djuth, and K. K. Shung, "Very high frequency (beyond 100 MHz) PZT kerfless linear arrays," *IEEE Trans. Ultrason., Ferroelectr., Freq. Control*, vol. 56, no. 10, pp. 2304–2310, Oct. 2009.
- [25] D. Certon, N. Felix, E. Lacaze, F. Teston, and F. Patat, "Investigation of cross-coupling in 1-3 piezocomposite arrays," *IEEE Trans. Ultrason., Ferroelectr., Freq. Control*, vol. 48, no. 1, pp. 85–93, Jan. 2001.



Tomasz Zawada received the M.Sc. degree in electronic engineering and the Ph.D. degree in micro-electronic engineering from the Wrocław University of Technology, Wrocław, Poland, in 2000 and 2004, respectively, and the MBA degree in management of technology from the Technical University of Denmark, Kongens Lyngby, Denmark, in 2012.

He was the Director of Engineering and Business Development with Meggitt Sensing Systems, Kvistgaard, Denmark. He has more than 15 years of experience in academic and industrial research in the fields of ceramic microsystems, microfluidics, and piezoelectric materials and devices. He co-founded TOOsonix A/S, Hørsholm, Denmark, where he is currently the Managing Director. He has authored or coauthored more than 70 scientific publications and reports, and holds six patents. His current research interests include applications of piezoelectric materials in sensors, transducers, and energy harvesting.



Louise Møller Bierregaard received the M.Sc. degree in physics and nanotechnology from the Technical University of Denmark (DTU), Kongens Lyngby, Denmark, in 2011.

She was involved in several MEMS Projects including energy harvesting and the fabrication of micro direct methanol fuel cells with DTU. In 2011, she joined Meggitt A/S, Kvistgaard, Denmark, as a Senior Research Engineer, where she was involved in energy harvesting and ultrasonic devices. Her current research interests include processing of PZT thick films and development of piezoelectric materials and devices.



Erling Ringgaard received the M.Sc. degree in chemistry and the Ph.D. degree in materials science from the Technical University of Denmark, Kongens Lyngby, Denmark, in 1994 and 1999, respectively.



Ruichao Xu received the B.Sc. degree and the M.Sc. degree in applied physics from the Technical University of Denmark, Kongens Lyngby, Denmark, in 2007 and 2009, respectively, and the Ph.D. degree in the field of PZT-based MEMS devices with special focus on energy harvesting for microsystems, under the supervision of Prof. Hansen, from the Department of Microtechnology and Nanotechnology, Technical University of Denmark, in 2012.



Michele Guizzetti was born in Italy in 1981. He received the Electronics Engineering degree and the Ph.D. degree in electronic instrumentation with a focus on power harvesting and autonomous systems from the University of Brescia, Brescia, Italy, in 2006 and 2010, respectively.



Franck Levassort was born in Paris, France. He received the bachelor's degree in applied physics and the DEA (M.Sc.) degree in physical acoustics from University Paris 7-Denis Diderot, Paris, in 1990 and 1991, respectively, and the Ph.D. degree in ultrasound from the University François-Rabelais of Tours, Tours, France, in 1996.

From 1997 to 2013, he was an Assistant Professor and since 2014, he has been a Full Professor of Electrical Engineering with the Institute of Technology, University François-Rabelais, Blois, France.

Since 2016, he has been a Deputy Director of GREMAN, Tours, a laboratory of more than 100 in the field of materials, microelectronics, acoustics, and nanotechnology. His current research interests include design, modeling, and characterization of piezoelectric composite materials and structures, as well as transducers for imaging applications.



Dominique Certon received the M.Sc. degree in signal processing and electrical engineering from the University of Orléans, Orléans, France, in 1991, and the Ph.D. degree and the Habilitation à diriger les recherches degree in applied acoustics and materials engineering from the University of Tours, Tours, France, in 1994 and 2010, respectively.

He is currently an Associate Professor of Telecommunication Systems with the University of Tours. He has authored or coauthored more than 50 communications and publications. His current research

interests include ultrasound probes for medical imaging based on capacitive micromachined transducers and piezoelectric technology.

Dr. Certon is a member of the French Society of Acoustics.